ASM Handbook, Volume 4A, *Steel Heat Treating Fundamentals and Processes*
J. Dossett and G.E. Totten, editors

Austenitizing in Steels

John G. Speer, Advanced Steel Processing and Products Research Center, Colorado School of Mines
Robert J. Gaster, Deere & Company, Moline Technology Innovation Center

Introduction

Austenite is the intermediate starting microstructure in many steels, which transforms during later processing or heat treatment to the microstructure desired in the particular steel alloy of interest. *Austenitization* refers to heating into the austenite phase field, during which the austenite structure is formed. Austenite is the high-temperature, face-centered cubic form of iron, stable at intermediate temperatures on the iron-carbon binary phase diagram. The austenitizing heat treatment almost always involves heating, but austenite formation also occurs during direct processing from very high temperature. For example, some newer processes involve casting and solidification directly linked with processing in the solid state, where austenite forms following solidification and transforms to the final microstructure before the steel is first cooled to room temperature. Such processes are not the focus of this article, but many of the principles related to austenitizing heat treatments are also applicable to austenite behavior during direct casting processes.

The iron-carbon equilibrium phase diagram, shown in Fig. 1, is a good starting point from which to consider austenite formation in steels. While the Fe-Fe_3C (cementite) diagram (shown using solid lines in Fig. 1) represents conditions that are metastable with respect to the true equilibrium in the iron-carbon system (where graphite is thermodynamically stable), cementite is the carbon-rich phase that is present in most commercial steels. Heating a ferrous alloy into the austenite phase field is associated with a thermodynamic driving force for austenite to replace the starting microstructure, which typically may contain ferrite, pearlite, iron carbide or cementite (Fe_3C), bainite and/or martensite, and perhaps some austenite that may have been present in the starting microstructure. Such austenite is referred to as retained austenite, resulting from incomplete transformation/decomposition during cooling from a previous processing step or sequence of steps.

Purposes and Overview of Austenitization

Steels are heated into the austenitic regime for a variety of purposes. In heat treating, austenite is formed to modify the microstructure, replacing an earlier-formed structure with a new microstructure tailored for the end use or next step in processing, via subsequent transformation at a lower temperature. For steels that are hot worked by means of rolling or forging, austenitization occurs as part of the reheating process to reduce the strength of the steel so that hot working can be accomplished with reasonable force or power inputs. Chemical homogenization can also be attained by increasing atomic mobility at high temperatures within the austenitic regime, although the kinetics of substitutional alloy redistribution are sluggish in the solid state, so homogenization may be limited in practice. However, interstitial homogenization of carbon in steels occurs more quickly, enabling the success of structure modifications in heat treatment of steels.

Partial austenitization is also employed intentionally during heat treating of some steels. For example, intercritical annealing (heating between the lower and upper critical temperatures for a particular steel, that is, between the A_1 and A_3 temperatures indicated in Fig. 1) of hypoeutectoid steels in the ferrite-plus-austenite two-phase field is used to generate intercritical ferrite in high-strength sheet products along with harder products of austenite decomposition, such as martensite in dual-phase microstructures. In hypereutectoid steels, for example, grade 52100, heating is often into the austenite-and-cementite two-phase field, whereby the presence of cementite moderates the austenite carbon concentration prior to quenching and enhances wear resistance in ball-bearing applications.

Austenitizing may involve plain carbon or low-alloy steels, where the transformations that occur upon heating primarily involve ferrite transformation and dissolution of cementite, or higher alloy steels where full or partial dissolution of alloy carbides or nitrides may be important. The starting microstructure also influences the austenitizing response, because the scale of the microstructure influences the distances over which solute diffusion may be required, and additional processes such as tempering or recrystallization can occur during heating of steels that are martensitic or cold worked before austenitizing. Alloy content of the steel can also influence austenitizing response, because carbide-forming elements will delay the diffusion of solute carbon in rapid heating conditions such as induction hardening. Reactions with the external environment may be an additional consideration, because oxidation and scale formation occur during heating, and carburizing or nitriding reactions and so on may also occur in the austenitic regime.

While heat-transfer considerations are not the focus of this article, it should be recognized that the microstructure evolution mechanisms that occur during austenitizing are diffusional, so temperature and time have a profound influence on the austenitizing response. Heating timeframes may range from fractions of a second (in surface-hardening applications such as induction hardening) to many hours for soaking of heavy sections. Temperature gradients influence microstructure development and hot working behavior and are sometimes inherent and intentional in processing, but in most cases are minimized through careful control of heating and soaking. Commercial software is available to calculate heat-transfer characteristics and thermal behaviors during heating.

Thermodynamics and Kinetics of Austenite Formation

Selection of Austenitizing Temperature. The presence of austenite at equilibrium can be predicted by using the phase diagram, such as in Fig. 1 for iron-carbon binary alloys, or by using thermodynamic databases for multicomponent steels. In practice, austenite formation may occur under conditions that may deviate considerably from equilibrium. Figure 2

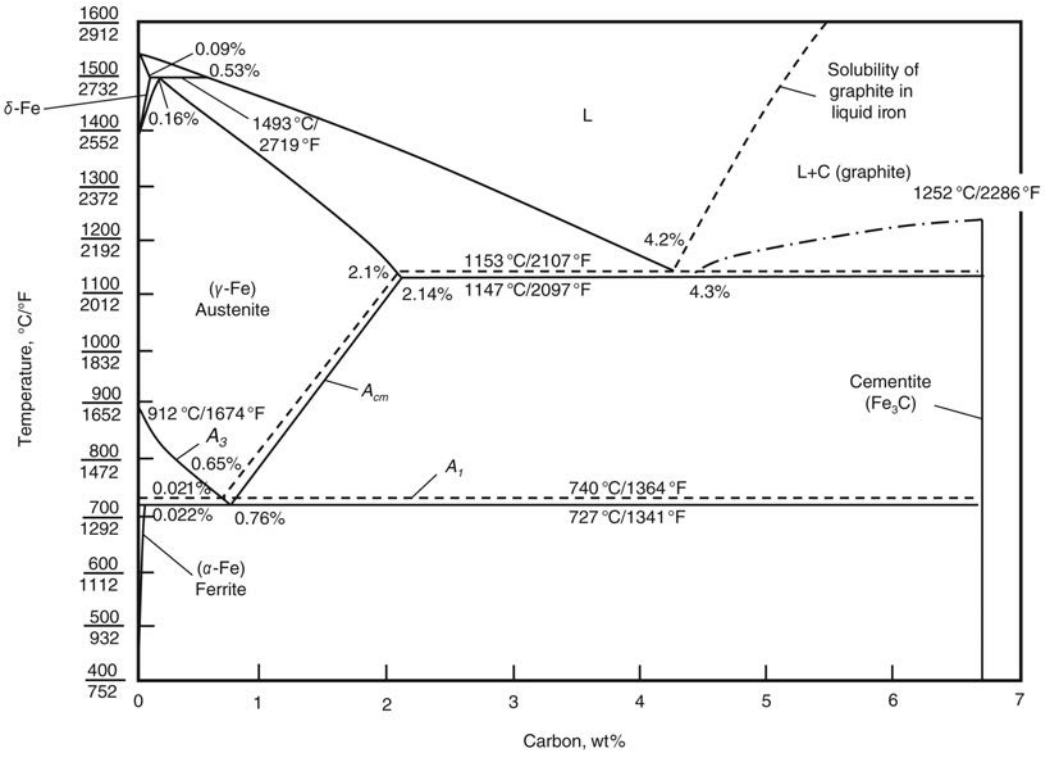

Fig. 1 Iron-carbon binary phase diagram, where solid lines indicate the metastable Fe-Fe_3C diagram and dashed lines are from the iron-graphite equilibrium diagram. Reprinted from Ref 1, adapted from Ref 2

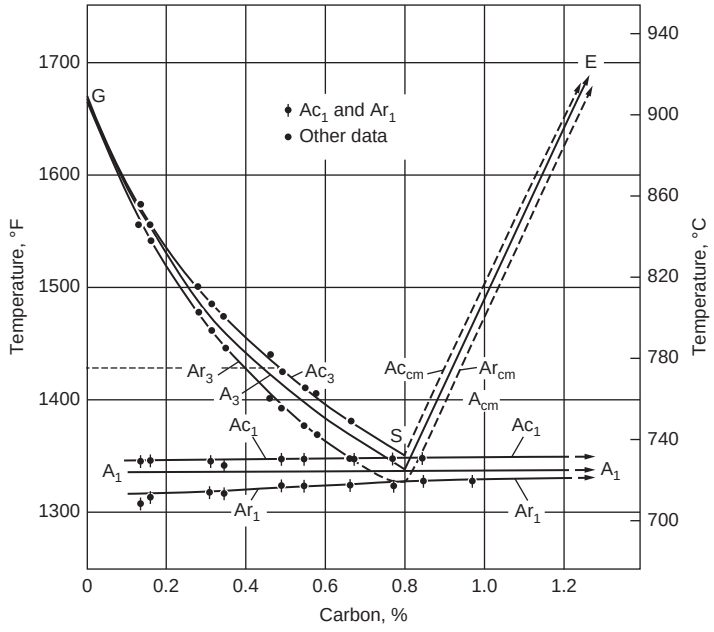

Fig. 2 Transformation temperatures from the phase diagram, along with critical temperatures for transformation during heating (c) or cooling (r) at 0.125 °C/min (0.225 °F/min). Reprinted from Ref 3

includes a portion of the iron-carbon phase diagram in the near-eutectoid region, with additional boundaries that illustrate the onset of transformation during heating or cooling. Some commonly employed heat treating nomenclature is associated with this figure, wherein the boundaries (as may be measured based on a thermal arrest) that define critical temperatures for transformation are designated as A_1 (critical temperature for eutectoid transformation), A_3 (critical temperature for primary ferrite transformation), and A_{cm} (critical temperature for primary cementite transformation). Additional subscripts of "c" or "r" are used to define the critical temperatures under heating or cooling conditions, respectively. The counterintuitive use of "c" as a subscript to describe heating rather than cooling stems from the French origin of these designations, wherein *chauffage* refers to heating and *refroidissement* to cooling. It should be noted that the information in Fig. 2 applies to iron-carbon binary alloys heated or cooled at 0.125 °C/min (0.225 °F/min), because the critical temperatures depend on both alloy composition and processing.

It is important to understand the critical temperatures to design appropriate heat treatment practices. For example, full austenitization is often the first step in heat treating, so the Ac_3 temperature for that particular steel must be exceeded to obtain the desired starting condition. In modern multicomponent steels, binary phase diagrams may not provide accurate information on critical temperatures and phase stability, however, due to the presence of other alloying elements. Commercial software packages are now available to obtain such information using computational thermodynamic databases. Experimental measurements using dilatometry are also employed to assess kinetic effects. Handbook summaries of critical temperatures can also be helpful, and Tables 1 and 2 show examples with recommended austenitizing and forging temperatures for a variety of carbon and low-alloy steels, respectively. Empirical equations are also available to

Table 1 Recommended austenitizing temperatures for several steels

Steel	Temperature, °C	Temperature, °F
Carbon steels		
1025	855–900	1575–1650
1030	845–870	1550–1600
1035	830–855	1525–1575
1037	830–855	1525–1575
1038(a)	830–855	1525–1575
1039(a)	830–855	1525–1575
1040(a)	830–855	1525–1575
1042	800–845	1475–1550
1043(a)	800–845	1475–1550
1045(a)	800–845	1475–1550
1046(a)	800–845	1475–1550
1050(a)	800–845	1475–1550
1055	800–845	1475–1550
1060	800–845	1475–1550
1065	800–845	1475–1550
1070	800–845	1475–1550
1074	800–845	1475–1550
1078	790–815	1450–1500
1080	790–815	1450–1500
1084	790–815	1450–1500
1085	790–815	1450–1500
1086	790–815	1450–1500
1090	790–815	1450–1500
1095	790–815(a)	1450–1500(b)
Free-cutting carbon steels		
1137	830–855	1525–1575
1138	815–845	1500–1550
1140	815–845	1500–1550
1141	800–845	1475–1550
1144	800–845	1475–1550
1145	800–845	1475–1550
1146	800–845	1475–1550
1151	800–845	1475–1550
1536	815–845	1500–1550
1541	815–845	1500–1550
1548	815–845	1500–1550
1552	815–845	1500–1550
1566	855–885	1575–1625
Alloy steels		
1330	830–855	1525–1575
1335	815–845	1500–1550
1340	815–845	1500–1550
1345	815–845	1500–1550
3140	815–845	1500–1550
4037	830–855	1525–1575
4042	830–855	1525–1575
4047	815–855	1500–1575
4063	800–845	1475–1550
4130	815–870	1500–1600
4135	845–870	1550–1600
4137	845–870	1550–1600
4140	845–870	1550–1600
4142	845–870	1550–1600
4145	815–845	1500–1550
4147	815–845	1500–1550
4150	815–845	1500–1550
4161	815–845	1500–1550
4337	815–845	1500–1550
4340	815–845	1500–1550
50B40	815–845	1500–1550
50B44	815–845	1500–1550
5046	815–845	1500–1550
50B46	815–845	1500–1550
50B50	800–845	1475–1550
50B60	800–845	1475–1550
5130	830–855	1525–1575
5132	830–855	1525–1575
5135	815–845	1500–1550
5140	815–845	1500–1550
5145	815–845	1500–1550
5147	800–845	1475–1550
5150	800–845	1475–1550
5155	800–845	1475–1550
5160	800–845	1475–1550
51B60	800–845	1475–1550
50100	775–800(c)	1425–1475(c)
51100	775–800(c)	1425–1475(c)
52100	775–800(c)	1425–1475(c)
6150	845–885	1550–1625
81B45	815–855	1500–1575
8630	830–870	1525–1600
8637	830–855	1525–1575
8640	830–855	1525–1575
8642	815–855	1500–1575
8645	815–855	1500–1575
86B45	815–855	1500–1575
8650	815–855	1500–1575
8655	800–845	1475–1550
8660	800–845	1475–1550
8740	830–855	1525–1575
8742	830–855	1525–1575
9254	815–900	1500–1650
9255	815–900	1500–1650
9260	815–900	1500–1650
94B30	845–885	1550–1625
94B40	845–885	1550–1625
9840	830–855	1525–1575

(a) Commonly used on parts where induction hardening is employed. All steels from SAE 1030 up may have induction hardening applications. (b) This temperature range may be employed for 1095 steel that is to be quenched in water, brine, or oil. For oil quenching, 1095 steel may alternatively be austenitized in the range 815 to 870 °C (1500 to 1600 °F). (c) This range is recommended for steel that is to be water quenched. For oil quenching, steel should be austenitized in the range 815 to 870 °C (1500 to 1600 °F). Reprinted from Ref 4

estimate critical temperatures based on alloy composition, and these can provide useful guidance for some low-alloy steels. For example, expressions of Andrews for Ac_3 and Ac_1 are reproduced as follows in Eq 1 and 2, respectively (Ref 6). (Some additional effects of manganese, chromium, copper, phosphorus, aluminum, arsenic, and titanium on Ac_3 are also mentioned in the original reference.)

$$Ac_3(°C) = 910 - 203\sqrt{C} - 15.2Ni + 44.7Si + 104V + 31.5Mo + 13.1W \quad \text{(Eq 1)}$$

$$Ac_1(°C) = 723 - 10.7Mn - 16.9Ni + 29.1Si + 16.9Cr + 290As + 6.38W \quad \text{(Eq 2)}$$

Both the tables and equations reflect the tendency for critical temperatures to increase with additions of austenite-stabilizing elements (such as carbon, nickel, manganese, etc.), which expand the temperature range of austenite stability, and for the critical temperature to decrease with additions of ferrite-stabilizing elements (such as silicon, chromium, and molybdenum), which expand the temperature range of ferrite stability.

The recommended temperature ranges in Table 1 reflect the need to fully austenitize while avoiding excessive austenite grain growth. The forging temperatures in Table 2 are higher for a given alloy, reflecting the desire to reduce the forming loads while also avoiding overheating, where incipient melting at grain boundaries or other embrittling mechanisms may be encountered. (The phase diagram in Fig. 1 shows that the liquidus temperature for austenite decreases with increasing carbon for most steels, consistent with the trends in Table 2.) Reheating temperatures before hot working may also reflect the need to control dissolution of precipitates in microalloyed high-strength low-alloy steels; this application is discussed in a later section. In a carburizing heat treatment, the temperature also controls the carbon mobility and maximum solubility in austenite. Finally, partial austenitizing heat treatments may apply to either hypoeutectoid or hypereutectoid steels, such as dual-phase sheet or ball-bearing steels, as mentioned previously. In these instances, the intercritical temperature (i.e., between the A_1 and A_3 or between the A_1 and A_{cm}) simultaneously controls both the austenite composition and the fraction of austenite and ferrite or carbide.

Table 2 Typical forging temperatures for various carbon and alloy steels

Steel	Major alloying elements	Typical forging temperature, °C	Typical forging temperature, °F
Carbon steels			
1010	...	1315	2400
1015	...	1315	2400
1020	...	1290	2350
1030	...	1290	2350
1040	...	1260	2300
1050	...	1260	2300
1060	...	1180	2160
1070	...	1150	2100
1080	...	1205	2200
1095	...	1175	2150
Alloy steels			
4130	Chromium, molybdenum	1205	2200
4140	Chromium, molybdenum	1230	2250
4320	Nickel, chromium, molybdenum	1230	2250
4340	Nickel, chromium, molybdenum	1290	2350
4615	Nickel, molybdenum	1205	2200
5160	Chromium	1205	2200
6150	Chromium, vanadium	1215	2220
8620	Nickel, chromium, molybdenum	1230	2250
9310	Nickel, chromium, molybdenum	1230	2250

Reprinted from Ref 5

Mechanisms and Kinetics of Austenite Formation. The initial microstructure influences the locations within the microstructure and the mechanisms by which austenite may form. Austenite nucleation is most likely to occur at interfaces, although the thermodynamic characteristics that apply to different interfaces are not necessarily identical. For example, nucleation would be possible at interfaces between pearlite colonies as soon as the

temperature exceeds the eutectoid or Ac_1, while there would not be a driving force for austenite nucleation at ferrite-ferrite interfaces (absent cementite) until much higher temperatures. In microstructures containing retained austenite, it may not be necessary for nucleation of austenite to occur, because the transformation could conceivably involve growth only of the existing austenite. Apart from the differences in nucleation behavior, the initial microstructure also influences the kinetics of austenite growth (Ref 7).

Austenite formation involves a change in crystal structure and composition. The crystal structure change is accomplished by short-range atom rearrangements at the interface, so that the body-centered cubic ferrite (or orthorhombic cementite) is transformed into face-centered cubic austenite. The kinetics of these structural rearrangements do not usually control the overall reaction kinetics, because long-range carbon and/or substitutional solute diffusion are needed to achieve the equilibrium austenite composition. The scale of (or dimensions associated with) the initial microstructure and carbon or solute distribution control the distance over which long-range diffusion occurs during austenitization and thus profoundly influence the kinetics (Ref 7). Coarse ferrite in combination with coarse alloy-enriched carbides represent the most sluggish austenitization kinetics, because the formation of homogeneous austenite requires dissolution of coarse carbides, involving redistribution of substitutional solutes, and carbon transport into the large volume previously consisting of carbon-depleted ferrite. On the other hand, martensitic or fully pearlitic starting microstructures contain the same overall solute content as the resulting austenite, so the transformation kinetics are less inhibited by the need for long-range solute transport. Fine eutectoid pearlite is a relatively simple case to consider, whereby austenite is stable just above the eutectoid temperature, and carbon redistribution is needed only on the scale of the pearlite interlamellar spacing.

The kinetics of isothermal austenite transformation from pearlite are shown schematically in Fig. 3. Here the eutectoid (pearlite) composition is indicated by the phase diagram on the left. The transformation kinetics are shown on the time-temperature-transformation (TTT) diagrams on the right. Above the eutectoid temperature, austenite formation occurs from pearlite, while below the eutectoid temperature, austenite decomposition occurs (forming pearlite in an appropriate temperature regime). The transformation start and completion lines are asymptotic to the dashed horizontal line at the eutectoid temperature, below which austenite is not stable and above which ferrite and cementite are not stable. At a given temperature, austenite formation from eutectoid pearlite has been shown to follow the well-known Johnson-Mehl-Avrami-Kolmogorov model (Ref 8, 9) that applies to many diffusional processes. Austenite formation in Fig. 3 occurs at shorter times with increasing temperature (i.e., the reaction rate increases monotonically with temperature) and exhibits a characteristic curve shape that is distinctly different than the usual C-curve kinetics that apply to austenite decomposition in the TTT diagram applicable below the eutectoid temperature. This distinctive characteristic arises from a fundamental difference between transformations that occur following heating and cooling. In transformations that occur following cooling, the free-energy change for the transformation (i.e., thermodynamic driving force) increases at lower temperatures, while atomic mobility is greater at higher temperatures, and the balance between these two factors leads to the well-known C-curve shape. In heating transformations, the free-energy change increases with increasing temperature, and the diffusion kinetics also increase with increasing temperature, so the reaction is always faster at higher temperatures.

The austenite growth rate is shown in Fig. 4, plotting austenite radius as a function of time, for different steels and temperatures. The slopes of the lines represent the interface velocity and increase at higher temperatures. Linear behavior indicates a constant interface velocity, which is possible in this special case where the eutectoid reaction is reversed ($\alpha + Fe_3C \rightarrow \gamma$), and the product inherits the entire carbon and alloy concentration of the parent pearlite. In the more general case where the parent microstructure is inhomogeneous and austenite grows with a different chemical composition (carbon-enriched austenite in hypoeutectoid steels, for example), growth under diffusion control becomes slower as the reaction proceeds and the solute concentration gradients are reduced, resulting in nonlinear behavior. Austenite transformation of pearlite can also occur, wherein the transformations of ferrite and carbide are uncoupled such that incompletely dissolved carbides can be present in the austenite. An example is shown in Fig. 5, where an austenite crystal is growing into pearlite in the central region of the micrograph. The austenite is light gray, having transformed to martensite at room temperature. Some undissolved carbides are clearly visible in the transformed volume, sometimes referred to as ghost pearlite (Ref 12). This behavior is more likely in rapid heating/short time situations such as in induction hardening. Eventually the carbides dissolve completely, given sufficient time and temperature in the single-phase austenite field, because the austenite composition becomes further carbon enriched.

Figure 6 shows the austenite carbon concentration in a hypereutectoid alloy versus log (time) for different austenitizing temperatures. The arrows indicate the point at which ferrite is completely transformed to austenite at each temperature, and the figure shows that the austenite carbon content continues to increase after this point, as carbide dissolution continues. Austenite

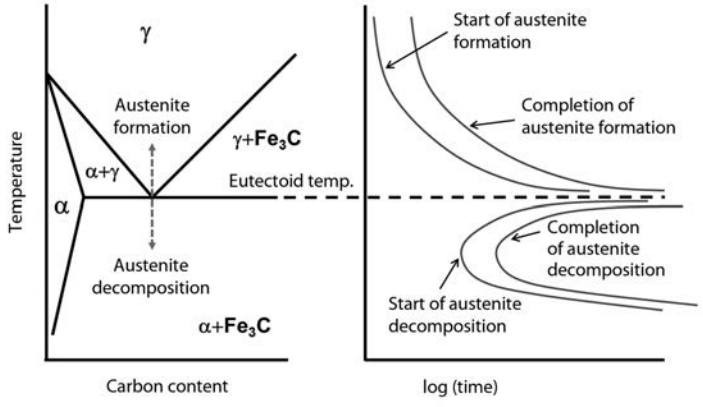

Fig. 3 Schematic iron-carbon phase diagram (left). Austenitization time-temperature diagram illustrating kinetics of isothermal austenite formation upon heating (upper right) and time-temperature-transformation diagram representing isothermal austenite decomposition upon cooling (lower right) for a eutectoid steel. Adapted from Ref 8

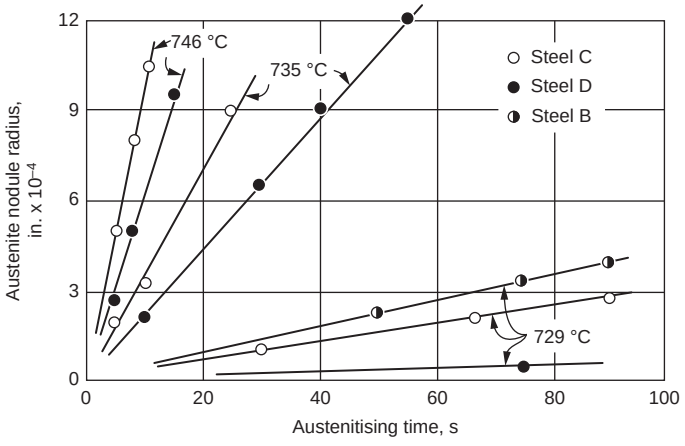

Fig. 4 Austenite grain (nodule) radius versus austenitizing time at different temperatures. Reprinted from Ref 1; original source Ref 10

formation and carbide dissolution are both faster at elevated temperature, and the equilibrium carbon concentration of the austenite increases with temperature up to the A_{cm} temperature. The decoupling of austenite growth from carbide dissolution is an important consideration, and aspects related to this behavior are sometimes reflected in TTT or time-temperature-austenitization (TTA) diagrams for specific steels.

The TTA diagram shown in Fig. 7 is for heating of a Ck 45 steel (similar to AISI 1045). This figure was adapted (Ref 12, 14–16) from the *Atlas zur Wärmebehandlung der Stähle*, which should serve as a useful reference on this topic. The light-gray Ac_2 line represents the Curie temperature below which the material is ferromagnetic. Superimposed on the temperature-time axes are also curves that reflect variations in heating rate over three orders of magnitude from 0.3 to 300 °C/s (0.54 to 540 °F/s). For this medium-carbon steel austenitized from a ferrite + partially spheroidized pearlite starting microstructure, Ac_1 represents the onset, while Ac_3 represents the completion of austenite formation. Austenite is likely to first consume the prior pearlite in this steel, because transformation of the low-carbon prior ferrite to austenite requires higher temperatures. Thus, carbide dissolution may be complete at the Ac_3, particularly at lower heating rates.

During and persisting for some time after carbide dissolution, an inhomogeneous carbon distribution may remain in the austenite until sufficient carbon transport has occurred across the dimensions of the starting microstructure. The inhomogeneous austenite composition may be reflected through a variation in the martensite start temperature during subsequent quenching of the austenite, wherein the presence of carbon-depleted regions leads to martensite formation at higher temperatures than in homogeneous austenite. The influences of time and temperature on austenite transformation kinetics are clearly illustrated in the figure, with austenite formation and homogenization completing at much lower temperatures under slower heating conditions. The presence and importance of inhomogeneous austenite is more relevant at high heating rates and short holding times during austenitization, such as may apply during induction hardening. While results as shown in Fig. 7 can be helpful, it should be reiterated that the positions and slopes of the curves are also dependent on prior processing and microstructure.

Austenite nucleation is likely to occur heterogeneously at pearlite colony interfaces or ferrite/carbide interfaces, although ferrite grain boundaries may also represent appropriate nucleation sites under some conditions (e.g., in pure iron or at high temperature). Austenite growth has been studied in low-carbon intercritically annealed sheet steels, where processing involves hot rolling and coil cooling (usually resulting in a ferrite + pearlite microstructure), followed by annealing in the ferrite + austenite two-phase field, and then quenching to transform the austenite to martensite and generate the dual-phase final microstructure (Ref 17). Manganese is commonly added to steels to provide hardenability.

Austenite nucleates first at the ferrite-pearlite interface and grows rapidly into pearlite, until pearlite dissolution is complete. After dissolution of pearlite, further growth of austenite into ferrite occurs, usually controlled by carbon diffusion in austenite. Because manganese partitions to austenite in preference to ferrite, final equilibration during intercritical annealing in the two-phase field involves an additional mechanism that does not usually apply during full austenitization of low-alloy steels at elevated temperature. Manganese partitioning is quite slow, so the final redistribution of manganese and adjustment of the phase fractions occurs over very long timeframes, which are not applicable to industrial processing.

Figure 8 shows a scanning electron micrograph of the partly transformed microstructure in a 0.06C-1.5Mn steel intercritically annealed for 1 h at 740 °C (1360 °F) and slow cooled to room temperature. The inhomogeneous distribution of austenite is clear, with a predominance of ferrite retained from the starting microstructure, and austenite distributed along the ferrite grain boundaries and triple points, having formed from pearlite. The ferrite is dark gray, while the austenite (transformed to martensite in this room-temperature micrograph) is lighter in contrast. The inset illustration shows the distribution of phases after air cooling in one of the austenite islands that formed during annealing. Here, martensite is present in the outer rim, while the austenite decomposed during slow cooling into ferrite and pearlite. This phase distribution is reflective of the hardenability effects of manganese enrichment in the outer rim of the austenite. This example provides an illustration of the spatial distribution of austenite as it begins to form in a ferrite + pearlite starting microstructure and important aspects of substitutional redistribution that can occur.

Figure 9 provides a TTA diagram for 100 Cr 6 steel (similar to AISI 52100) in a spheroidized condition. This is a hypereutectoid steel with a substantial chromium addition in which

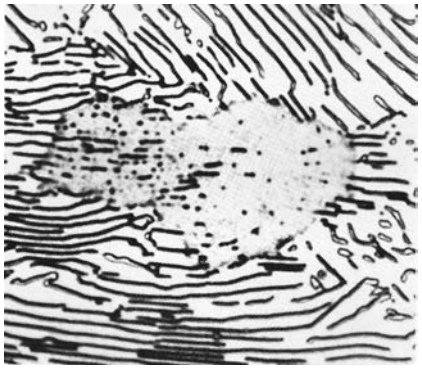

Fig. 5 Austenite formation in a eutectoid steel (0.81C, 0.07Si, 0.65Mn) held 26 s at 730 °C (1350 °F) and water quenched. Original magnification: 2000×. Reprinted from Ref 11

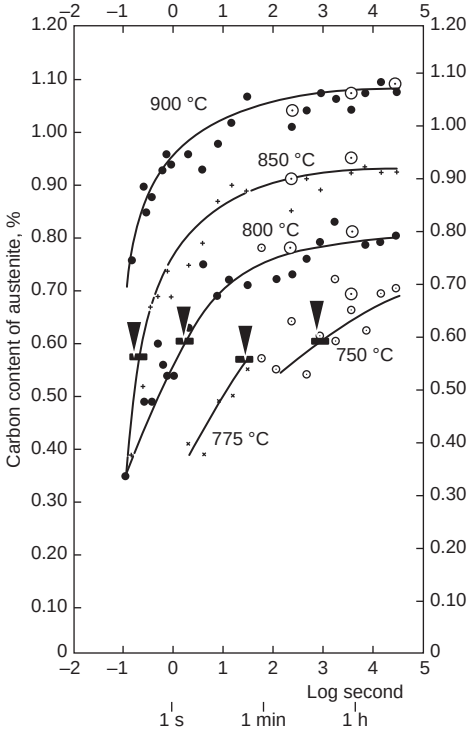

Fig. 6 Carbon content in austenite as a function of austenitizing time and temperature for a 1.27C (by weight) steel. Arrows indicate the disappearance of ferrite. Reprinted from Ref 13

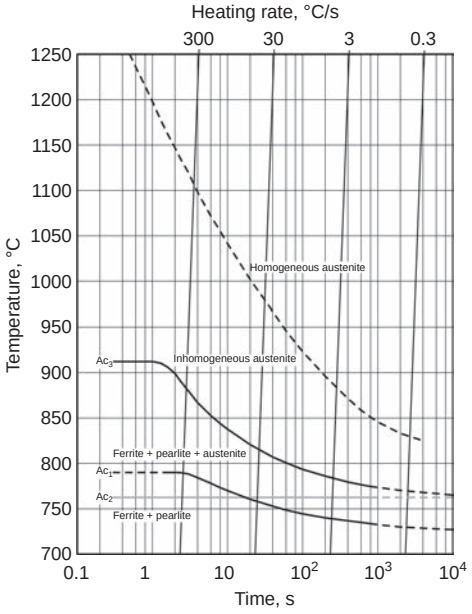

Fig. 7 Time-temperature-austenitization diagram for Ck 45 steel. Adapted from Ref 14 and 15 and reprinted from Ref 16

chromium is incorporated into the cementite, so additional considerations also apply in this steel, because carbides are stable with austenite over a range of temperatures in the intercritical regime during heating, and carbide dissolution and austenite homogenization involve slower diffusion of substitutional (chromium) atoms, as well as carbon. Here, Ac_{1b} indicates the beginning of austenite formation, where there is a driving force to transform the ferrite and dissolve some of the carbides while coarsening others. The end of ferrite transformation during heating is represented by Ac_{1e}, where the microstructure consists of austenite plus carbide. Carbide dissolution continues during further heating over a considerable range of temperatures up to the Ac_c, followed by redistribution of solute carbon and chromium during austenite homogenization.

The previous discussion considered some nonequilibrium effects related to the behavior of carbides during austenitizing. Nonequilibrium effects related to the behavior of ferrite during austenitizing also occur at rapid heating rates and short holding times, such as in induction hardening. Austenite formation in pure iron is partitionless, occurring without any carbon or solute transport, and only requires short-range atom movements to reconstruct a different lattice structure at the interface. The transformation temperature (Ac_3) is shown in Fig. 10 and varies only a small amount over a wide range of heating rates, much less in comparison to the alloys shown earlier in Fig. 7 and 9. Here, the ferrite is stable to much higher temperatures than the eutectoid temperature, so growth is very fast once the temperature is high enough that a driving force is available for transformation to austenite. (If the transformation was not fast, the temperature of transformation would be much higher at very fast heating rates.)

While commercial steels do not usually resemble pure iron, it should be recognized that large ferrite grains in the initial microstructure could exhibit behaviors similar to pure iron if they persist to high temperature without having transformed to austenite. The thermodynamics of partitionless decomposition of austenite during cooling are reasonably well understood, because such conditions apply to massive ferrite transformation as well as martensite transformation that represents the classic situation of transformation without a composition change. The concepts are not much discussed in the context of austenite formation during heating but may have applicability at high heating rates where transformation is suppressed at low temperatures, where partitionless transformation is impossible (Ref 7, 19).

The T_o concept is used to understand driving forces for partitionless transformation and is illustrated in Fig. 11. The free energies of ferrite and austenite are shown in the upper portion as a function of carbon concentration for a temperature T_1 on the phase diagram (below); the common tangent to the free-energy curves defines the equilibrium ferrite and austenite compositions on the phase diagram. The intersection between the ferrite and austenite free-energy curves is designated T_o and lies between the equilibrium ferrite and austenite compositions, within the $\alpha + \gamma$ phase field. While the T_o does not represent equilibrium, it represents the locus of compositions and temperatures above which austenite has a lower free energy than ferrite of the same chemical composition and below which ferrite has a lower free energy than austenite. While under equilibrium transformation conditions, the temperature must exceed the A_3 curve to obtain full austenitization; under partitionless conditions there is actually a driving force for austenite to replace ferrite of the same composition once the T_o temperature is reached.

For low carbon levels applicable to ferrite, the T_o temperature is very high, so partitionless austenite formation could occur very quickly. Equally important, rapid partitionless transformation during cooling may also occur if short austenitizing times do not permit homogenization of austenite. The significance of this discussion lies in its potential application to austenite formation at rapid heating rates and short holding times in microstructures containing coarse ferrite (along with coarse pearlite, for example), such as may apply during induction hardening. Here, rapid forward and rapid reverse transformation from ferrite to austenite and then to ferrite again may occur under partitionless conditions, wherein the final microstructure containing low-carbon ferrite has the appearance of incomplete austenitization with untransformed ferrite but in fact resulted from full austenitization without homogenization of carbon in the austenite.

Austenite Grain Growth

The desired grain size of the austenite that forms during austenitization is dependent on the application. Coarse austenite grains increase hardenability, although in practice, alloying is used to control hardenability, because finer austenite is usually preferred to refine the final microstructure, enhancing strength and toughness. Due to grain growth or grain coarsening, the austenite grain size is expected to increase with time or temperature, as shown for pure

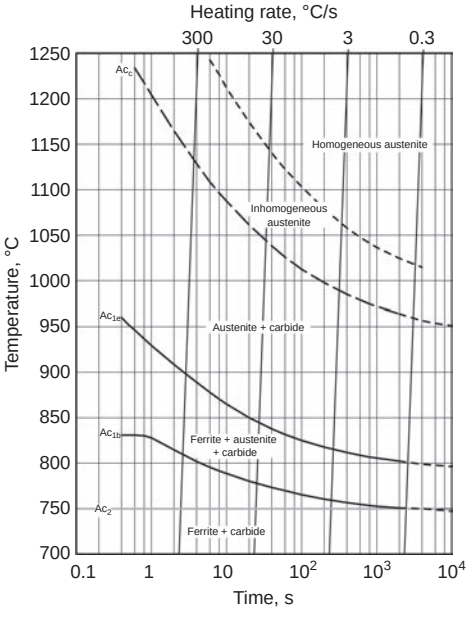

Fig. 9 Time-temperature-austenitization diagram for 100 Cr 6 steel with a ferrite + spheroidized carbide initial microstructure. Adapted from Ref 14 and 15 and reprinted from Ref 16

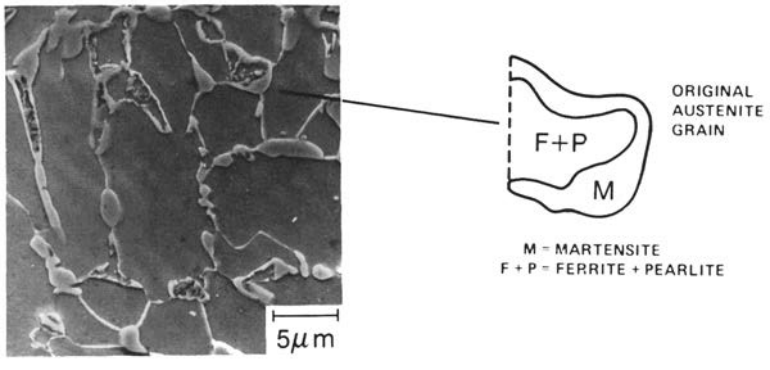

Fig. 8 Microstructure of 0.06C-1.5Mn steel intercritically annealed 1 h at 740 °C (1360 °F) and then slow cooled. Reprinted from Ref 17

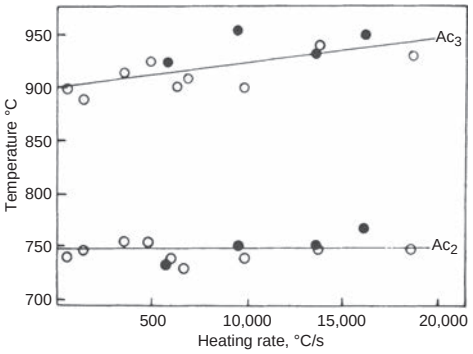

Fig. 10 Effect of heating rate on the temperature at which ferrite transforms to austenite (Ac_3) in pure iron. The Curie temperature is also shown (Ac_2). Reprinted from Ref 18

iron in Fig. 12. In alloys, the austenite grain-coarsening behavior may be different, because alloying elements in solution or in the form of precipitates may retard grain growth by means of solute drag or precipitate pinning effects, respectively, on austenite grain-boundary motion. The pinning precipitates in many steels are aluminum nitrides, AlN, and provide effective grain refinement at low temperatures in the austenite phase field during heat treatments such as normalizing, carburizing, and so on. Aluminum is added to many steels to remove oxygen from the liquid prior to casting and combines with solute nitrogen to form aluminum nitrides during cooling or reheating. The aluminum fine-grained practice is therefore available to suppress grain growth in many steels during subsequent reaustenitizing.

Figure 13 shows the ASTM International grain size number for austenite as a function of heating (austenitizing) temperature for steels that would be produced with and without an aluminum deoxidizing treatment during steelmaking, the so-called fine-grained or coarse-grained practice, respectively. Note that smaller ASTM International grain size numbers represent coarser grains. In the aluminum-free coarse-grained steel, austenite grain size increases continuously with temperature. In the aluminum-added fine-grained steel, the austenite grains are pinned by AlN, and the grain size remains small up until the grain-coarsening temperature. (Other precipitates, such as vanadium nitride or niobium carbide, can also be effective at suppressing grain coarsening during reaustenitizing. See Ref 22 and 24.) A sudden increase in grain-growth kinetics occurs at the grain-coarsening temperature, accompanied by abnormal coarsening where some grains grow much larger than the others, leading to grain sizes that may be coarser than would be observed in steels without any grain-refining additive. At still higher austenitizing temperatures, the pinning particles coarsen and lose effectiveness, so normal grain growth resumes, and austenite grain sizes are similar to the steels without grain-refining additions (Ref 22).

Because the austenite grain size has an important influence on the final microstructure and properties for a given application, it is often desirable to measure the prior-austenite grain size. The term *prior austenite* is used because the austenite grains that existed at high temperature are no longer present, having transformed to a different microstructure at room temperature. Evidence for the location of the prior-austenite grain boundaries can be readily obtained in some microstructures using careful metallographic techniques (and specialized etchants), particularly in fully martensitic microstructures (because the martensite plates/packets grow within a single austenite grain and do not cross the austenite boundaries) or in partially transformed microstructures where a specific transformation product "decorates" the prior-austenite boundaries, having nucleated only on those boundaries during transformation. In other instances, such as in low-carbon ferritic microstructures, it can be very difficult to bring out the prior-austenite microstructure. Special processing can aid in rendering the prior-austenite microstructure, to help characterize the austenitizing response of a particular steel. For example, controlled cooling may be applied to generate a transformation product located predominantly at the prior boundaries, and carburizing may be used to generate a network of cementite at the austenite grain boundaries, which remains in the microstructure after transformation during cooling (Ref 25).

Control of Solute Concentrations in Austenite

While precipitates are helpful for austenite grain-size control in many heat treatments, there are other applications where certain precipitates must be dissolved in austenite for the solutes to have their desired effect. Examples include boron-containing martensitic steels, and microalloyed high-strength low-alloy (HSLA) steels. In the boron-added steels, solute boron segregates to austenite grain boundaries and provides substantially enhanced hardenability for typical austenitizing treatments, at optimum boron levels of 10 or 20 (weight) ppm. Boron is a strong nitride former, so titanium is often added (in excess of the nitrogen concentration) to prevent BN precipitation, because boron is only effective when present in solution. An iron borocarbide phase can also form, however, so austenitizing times and temperatures must also take into consideration the precipitation kinetics of $Fe_{23}(C,B)_6$ in these steels (Ref 26).

Microalloyed HSLA steels are most often subjected to thermomechanical processing as part of hot working in the austenitic regime, modifying the final microstructure and properties. Here, small additions of niobium, for example, are added to suppress austenite recrystallization at low temperatures in the austenitic hot working regime during finish rolling, forging, and so on. The deformed ("pancaked") unrecrystallized austenite is associated with increased austenite grain-boundary surface area, which enhances nucleation during transformation, leading to a finer microstructure and increased strength and toughness. The key mechanisms involve microalloy carbide precipitation on the austenite grain boundaries and deformation substructure (sub-boundaries) during thermomechanical processing; the precipitates pin the boundaries and suppress

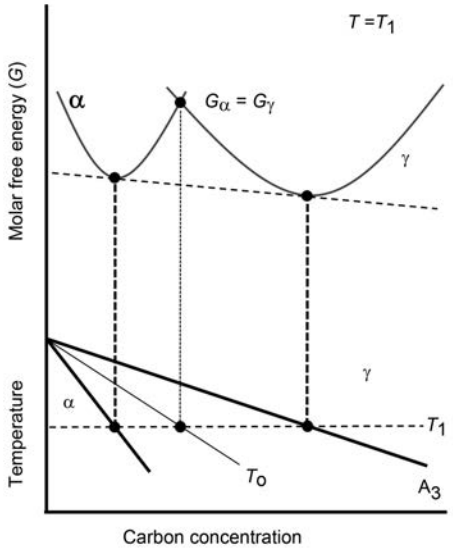

Fig. 11 Schematic illustration of the thermodynamic origin of the T_o curve (above), where the free energies of austenite and ferrite are equal, overlaid on a portion of the iron-carbon phase diagram (below). The equilibrium ferrite and austenite (A_3) compositions are given by the common tangent to the respective free-energy curves. Adapted from Ref 20

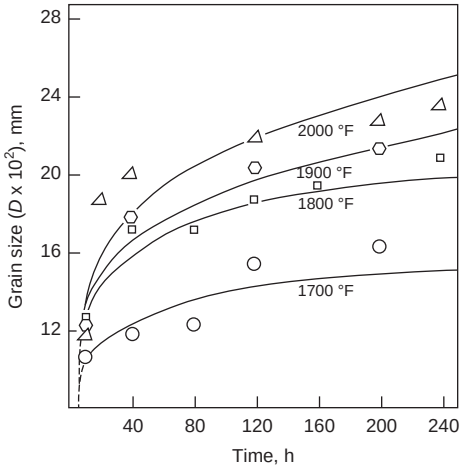

Fig. 12 Austenite grain size of pure iron as a function of austenitizing time and temperature, showing expected grain-growth behavior. Reprinted from Ref 8; original source Ref 21

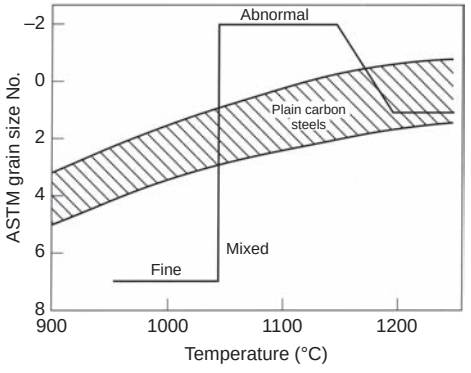

Fig. 13 Schematic illustration showing effect of austenitizing temperature on austenite grain size of plain carbon coarse-grained (shaded area) and fine-grained steels (solid line). The ASTM International grain size number "N" is defined by the relation $2^{N-1} = n$, where n is the number of grains/in.^{2} at 100× magnification. Reprinted from Ref 22; see also Ref 23

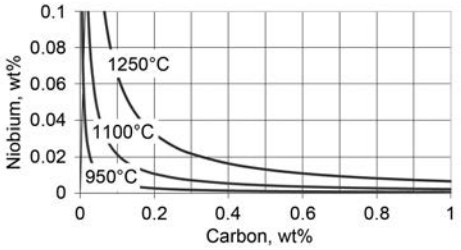

Fig. 14 Niobium carbide solubility isotherms for austenite at 950, 1100, and 1250 °C (1740, 2010, and 2280 °F)

recrystallization. For this mechanism to operate, the microalloy carbide solubility must be controlled carefully, because the carbides must be dissolved in the austenite during reheating prior to hot working and then must precipitate at lower temperatures within the hot-working regime. If the precipitates remain undissolved during reheating, they do not contribute beneficially to the thermomechanical processing response. (This mechanism should not be confused with the fine-grained practice discussed earlier, where precipitates that remain undissolved during austenitizing as part of heat treating, not hot working, help suppress austenite grain growth.)

The solubility of microalloying elements is reasonably well understood, and a variety of solubility product relationships are available in the literature for relevant carbides and nitrides (Ref 22). As an example, Fig. 14 shows solubility isotherms for niobium carbide in austenite, showing the strong dependence of NbC solubility on temperature, as well as concentrations of both carbon and niobium. The isotherms represent the loci of niobium and carbon solute concentrations in equilibrium with austenite, satisfying the solubility product expression in Eq 3, where the solute concentrations are in weight percent and the temperature is in Kelvin:

$$\log_{10}[\mathrm{Nb}][\mathrm{C}] = 2.26 - 6770/T \qquad \text{(Eq 3)}$$

For particular concentrations of carbon and niobium added to the steel, the solubility isotherms show whether or not all of the NbC is dissolved during reheating at the temperature of interest. If the niobium and carbon concentrations are below the solubility isotherm for a given temperature, then NbC can be fully dissolved in the austenite at that temperature. If the concentrations are above the solubility isotherm, then NbC precipitates should be present at equilibrium; the amount of NbC and the remaining niobium and carbon in austenite can be determined by applying appropriate mass-balance considerations (Ref 27). While these solubility considerations are critical in alloy and process designs for thermomechanical processing, they are also applicable in designing precipitation schemes to enhance suppression of austenite grain coarsening during heat treatment and have proved effective, for example, in enabling the use of increased carburizing temperatures to accelerate carbon transport without undesired coarsening of the microstructure (Ref 24).

ACKNOWLEDGMENTS

The sponsors of the Advanced Steel Processing and Products Research Center at Colorado School of Mines are gratefully acknowledged.

REFERENCES

1. F.C. Campbell, Ed., *Elements of Metallurgy and Engineering Alloys*, ASM International, 2008, p 153
2. T.B. Massalski, H. Okamoto, P.R. Subramanian, and L. Kacprzak, *Binary Alloy Phase Diagrams*, 2nd ed., ASM International, 1990, p 843
3. R.F. Mehl and C. Wells, Constitution of High-Purity Iron-Carbon Alloys, *Met. Technol.*, Vol 4 (No. 4), TP 798, June 1937, p 1–41
4. *Heat Treating*, Vol 4, *ASM Handbook*, ASM International, 1991, p 961
5. C.J. Van Tyne, Forging of Carbon and Alloy Steels, *Metalworking: Bulk Forming*, Vol 14A, *ASM Handbook*, ASM International, 2005, p 241–260; Cites original source: J.T. Winship, Fundamentals of Forging, *Am. Mach.*, July 1978, p 99–122
6. K.W. Andrews, Empirical Formulae for the Calculation of Some Transformation Temperatures, *JISI*, Vol 203, 1965, p 721–727
7. J.J. Coryell, D.K. Matlock, and J.G. Speer, The Effect of Induction Hardening on the Mechanical Properties of Steel with Controlled Prior Microstructures, *Heat Treating for the 21st Century: Vision 2020 and New Materials Development*, Materials Science and Technology (MS&T) 2005, p 3–14
8. C.R. Brooks, *Principles of the Austenitization of Steels*, Elsevier Applied Science, 1992
9. B.C. De Cooman and J.G. Speer, *Fundamentals of Steel Product Physical Metallurgy*, AIST, 2011, p 85–89
10. G.A. Roberts and R.F. Mehl, *Trans. ASM*, Vol 31, 1943, p 615
11. L.E. Samuels, *Optical Microscopy of Carbon Steels*, American Society for Metals, 1980, p 266
12. G. Krauss, *Steels: Processing, Structure and Performance*, ASM International, 2005
13. G. Molinder, A Quantitative Study of the Formation of Austenite and the Solution of Cementite at Different Austenitizing Temperatures for a 1.27% Carbon Steel, *Acta Metall.*, Vol 4, 1956, p 565–571
14. J. Orlich, A. Rose, and P. Wiest, Zeit-Temperatur-Austenitisierung-Schaubilder, *Atlas zur Wärmebehandlung der Stähle*, Band 3 (Vol 3), Verlag Stahleisen, 1973
15. J. Orlich and H.-J. Pietrzeniuk, Zeit-Temperatur-Austenitisierung-Schaubilder 2, Teil (Part 2), *Atlas zur Wärmebehandlung der Stähle*, Band 4 (Vol 4), Verlag Stahleisen, 1976
16. K. Clarke, "The Effect of Heating Rate and Microstructural Scale on Austenite Formation, Austenite Homogenization, and As-Quenched Microstructure in Three Induction Hardenable Steels," Ph.D. thesis, Colorado School of Mines, 2008
17. G.R. Speich, V. Demarest, and R.L. Miller, Formation of Austenite during Intercritical Annealing of Dual-Phase Steels, *Metall. Trans. A*, Vol 12, Aug 1981, p 1419–1428
18. W.L. Haworth and J.G. Parr, The Effect of Rapid Heating on the Alpha-Gamma Transformation in Iron, *Trans. ASM*, Vol 58, 1965, p 476–488
19. E.D. Schmidt, E.B. Damm, and S. Sridhar, A Study of Diffusion and Interface- Controlled Migration of the Austenite/ Ferrite Front during Austenitization of a Case-Hardenable Alloy Steel, *Metall. Mater. Trans. A*, Vol 38, April 2007, p 698–715
20. H.K.D.H. Bhadeshia, *Bainite in Steels*, 2nd ed., IOM Communications, 2001, p 9
21. H.B. Probst and M.J. Sinnott, *Trans. AIME*, Vol 203, 1955, p 215
22. T. Gladman, *The Physical Metallurgy of Microalloyed Steels*, The Institute of Materials, 1997
23. E.C. Bain, *Functions of the Alloying Elements in Steel*, American Society for Metals, 1939, p 137
24. K.A. Alogab, D.K. Matlock, J.G. Speer, and H.J. Kleebe, The Influence of Niobium Microalloying on Austenite Grain Coarsening Behavior of Ti-Modified SAE 8620 Steel, *ISIJ Int.*, Vol 47, 2007, p 307–316
25. H.W. McQuaid, The McQuaid-Ehn Test, *Metals Handbook*, American Society for Metals, 1948, p 407–408
26. K.A. Taylor and S.S. Hansen, The Boron Hardenability Effect in Thermomechanically Processed, Direct-Quenched 0.2 Pct. C Steels, *Metall. Trans. A*, Vol 21, June 1990, p 1697–1708
27. J.G. Speer, J.R. Michael, and S.S. Hansen, Carbonitride Precipitation in Niobium/ Vanadium Microalloyed Steels, *Metall. Trans. A*, Vol 18, 1987, p 211–222